A Metagenomic Survey of Microbes in Honey Bee Colony Collapse Disorder
Diana L. Cox-Foster, *et al.*
Science **318**, 283 (2007);
DOI: 10.1126/science.1146498

alent force analysis on junction *BR* (Fig. 2E, 2F, Table 1). Junction *BR* exhibited much reduced (by a factor of five or six) force dependence of the equilibrium populations compared with junctions *XR* and *HR* (compare Δx_{eq} values in Table 1). The residual force dependence of the equilibrium populations may be attributed to the finite diameter of the DNA duplex (*18*). In contrast to junctions *XR* and *HR*, application of force on junction *BR* accelerated both forward and backward transitions (Fig. 2F). Therefore, the distance between the ends of the B and R arms, d_{BR}, must be larger in the transition state than in the stacked-X structures. This condition is satisfied only if ϕ_{II} in the transition state is smaller than the 40° of the stacked-X structure. Furthermore, the distance to the transition state is 0.37 nm at minimum, which constrains ϕ_{II} to be essentially zero (*18*). In combination, our best estimate is $(\phi_{II}, \psi_{II})_{ts}$ = (0°, 70°) for *ts*II (Fig. 3C). This transition state is similar to the open state, but with arms deviating by about 20° from the ideal open state while displaying signatures on which pairs of helices are nearly stacked over each other (Fig. 3D). The structure bears a strong resemblance to the HJ structure bound to the Cre recombinase (*24*). Following the same argument, we can deduce that the transition state in the *iso*I-like conformational space, *ts*I, also has $(\phi_I, \psi_I)_{ts}$= (0°, 70°).

By probing the HJ dynamics in response to pulling forces in three different directions, we mapped the location of the transition states in the two-dimensional (2D) reaction landscape and deduced the global structure of the transient species populated during the HJ conformational changes. Our simplest model envisions a shallow minimum between the two transition states, depicted as the open structure (Fig. 3A and 3D), but it is also possible that a continuum of conformations exist, spanning from *ts*I and *ts*II with nearly identical free energies, instead of having a single well-defined minimum.

The development reported here expands on the current arsenal of hybrid single-molecule techniques combining force and other observables (*8*, *25*–*27*). Unlike DNA or RNA hairpins, where forces on the order of 15 pN are necessary to induce mechanical unzipping (*10*, *11*), the conformations of HJs could be biased at 0.5 pN or lower. The lever-arm effect makes it unlikely that a purely mechanical tool could have probed the force effect on HJ conformations, because if the arms are lengthened to magnify the distance change, the force effect will occur at even lower forces. FRET can also report on vectors other than the end-to-end distances, which we exploited here by pulling on *XR*, *HR*, or *BR* arms while simultaneously measuring the same HB vector by FRET, which led to the 2D mapping of reaction landscapes. Our method is readily applicable to other nucleic acids systems and their interaction with proteins and enzymes, and with the advent of new orthogonal labeling techniques, should be extendable to proteins and protein complexes. The next technical challenge would be to obtain time evolution of the end-to-end distance by force, for example, due to the action of DNA processing enzymes (*28*), and correlate it with the enzyme conformational changes simultaneously measured by fluorescence.

References and Notes

1. C. Bustamante, Y. R. Chemla, N. R. Forde, D. Izhaky, *Annu. Rev. Biochem.* **73**, 705 (2004).
2. L. Stryer, R. P. Haugland, *Proc. Natl. Acad. Sci. U.S.A.* **58**, 719 (1967).
3. T. Ha *et al.*, *Proc. Natl. Acad. Sci. U.S.A.* **93**, 6264 (1996).
4. T. Ha, *Methods* **25**, 78 (2001).
5. A. Ashkin, J. M. Dziedzic, J. E. Bjorkholm, S. Chu, *Opt. Lett.* **11**, 288 (1986).
6. A. N. Kapanidis *et al.*, *Science* **314**, 1144 (2006).
7. S. C. Blanchard, R. L. Gonzalez, H. D. Kim, S. Chu, J. D. Puglisi, *Nat. Struct. Mol. Biol.* **11**, 1008 (2004).
8. M. J. Lang, P. M. Fordyce, S. M. Block, *J. Biol.* **2**, 6 (2003).
9. P. B. Tarsa *et al.*, *Angew. Chem. Int. Ed. Engl.* **46**, 1999 (2007).
10. J. Liphardt, B. Onoa, S. B. Smith, I. Tinoco, C. Bustamante, *Science* **292**, 733 (2001).
11. M. T. Woodside *et al.*, *Science* **314**, 1001 (2006).
12. R. Holliday, *Genet. Res.* **5**, 282 (1964).
13. D. R. Duckett *et al.*, *Cell* **55**, 79 (1988).
14. D. M. J. Lilley, *Q. Rev. Biophys.* **33**, 109 (2000).
15. B. F. Eichman, J. M. Vargason, B. H. M. Mooers, P. S. Ho, *Proc. Natl. Acad. Sci. U.S.A.* **97**, 3971 (2000).
16. R. J. Grainger, A. I. H. Murchie, D. M. J. Lilley, *Biochemistry* **37**, 23 (1998).
17. Materials and methods are available as supporting material on *Science* Online.
18. S. A. McKinney, A. C. Declais, D. M. J. Lilley, T. Ha, *Nat. Struct. Biol.* **10**, 93 (2003).
19. J. C. Meiners, S. R. Quake, *Phys. Rev. Lett.* **84**, 5014 (2000).
20. I. Rasnik, S. A. McKinney, T. Ha, *Nat. Methods* **3**, 891 (2006).
21. S. A. McKinney, C. Joo, T. Ha, *Biophys. J.* **91**, 1941 (2006).
22. C. Bustamante, J. F. Marko, E. D. Siggia, S. Smith, *Science* **265**, 1599 (1994).
23. J. Yu, T. Ha, K. Schulten, *Nucleic Acids Res.* **32**, 6683 (2004).
24. G. D. Van Duyne, *Annu. Rev. Biophys. Biomol. Struct.* **30**, 87 (2001).
25. A. Ishijima *et al.*, *Cell* **92**, 161 (1998).
26. H. Shroff *et al.*, *Nano Lett.* **5**, 1509 (2005).
27. J. Gore *et al.*, *Nature* **439**, 100 (2006).
28. J. B. Lee *et al.*, *Nature* **439**, 621 (2006).

29. We thank W. Cheng at University of California–Berkeley for providing the protocol for the preparation of anti-Dig coated bead, M. Wang at Cornell University for giving generous advice about building optical tweezers, Y. Chemla at University of Illinois for helpful discussion, and C. Joo for generous help in preparation of illustrations. Funding was provided by the National Sciences Foundation CAREER Award (PHY 0134916) and the National Institutes of Health (GM065367). T.H. is an investigator with the Howard Hughes Medical Institute.

5 June 2007; accepted 11 September 2007
10.1126/science.1146113

A Metagenomic Survey of Microbes in Honey Bee Colony Collapse Disorder

Diana L. Cox-Foster,[1] Sean Conlan,[2] Edward C. Holmes,[3,4] Gustavo Palacios,[2] Jay D. Evans,[5] Nancy A. Moran,[6] Phenix-Lan Quan,[2] Thomas Briese,[2] Mady Hornig,[2] David M. Geiser,[7] Vince Martinson,[8] Dennis vanEngelsdorp,[1,9] Abby L. Kalkstein,[1] Andrew Drysdale,[2] Jeffrey Hui,[2] Junhui Zhai,[2] Liwang Cui,[1] Stephen K. Hutchison,[10] Jan Fredrik Simons,[10] Michael Egholm,[10] Jeffery S. Pettis,[5] W. Ian Lipkin[2]*

In colony collapse disorder (CCD), honey bee colonies inexplicably lose their workers. CCD has resulted in a loss of 50 to 90% of colonies in beekeeping operations across the United States. The observation that irradiated combs from affected colonies can be repopulated with naive bees suggests that infection may contribute to CCD. We used an unbiased metagenomic approach to survey microflora in CCD hives, normal hives, and imported royal jelly. Candidate pathogens were screened for significance of association with CCD by the examination of samples collected from several sites over a period of 3 years. One organism, Israeli acute paralysis virus of bees, was strongly correlated with CCD.

Methods for cloning nucleic acids of microbial pathogens directly from clinical and environmental specimens afford unprecedented opportunities for pathogen discovery and surveillance. Subtractive cloning, polymerase chain reaction (PCR), and DNA microarrays have implicated previously unknown pathogens as the etiological agents of several acute and chronic diseases. Here, we describe the application of unbiased high-throughput pyrosequencing technology (*1*) in the characterization of the microflora associated with *Apis mellifera* in a search for the cause of colony collapse disorder (CCD).

CCD is characterized by the rapid loss from a colony of its adult bee population (*2*–*4*). No dead adult bees are found inside or in close proximity to the colony. At the final stages of collapse, a queen is attended only by a few newly emerged adult bees. Collapsed colonies often have considerable capped brood and food reserves. The phenomenon of CCD was first reported in 2006;

however, beekeepers noted unique colony declines consistent with CCD as early as 2004. An estimated 23% of beekeeping operations in the United States suffered from CCD over the winter of 2006–2007. These beekeepers lost an average of 45% of their operations (*5*). Since the introduction of the varroa mite in the late 1980s, colonies have experienced increased mortality; however, in contrast to CCD, these colony deaths are marked by dead bees in the hive, an incremental decline in worker population, and robbing and pest invasion. One hypothesis is that CCD is due to the introduction of a previously unrecognized infectious agent. This idea is supported by preliminary evidence that CCD is transmissible through the reuse of equipment from CCD colonies and that such transmission can be broken by irradiation of the equipment before use (*6*).

Bees were analyzed in a metagenomic survey of four widely separated operations across the United States that were affected by CCD. All of the operations were migratory, with wintering yards in either Florida or California in February 2007 (fig. S1) (*7*). Two non-CCD samples were collected from Hawaii and Pennsylvania. An additional sample of apparently healthy bees imported from Australia and four samples of imported royal jelly from China were also tested as potential sources of pathogens. Total RNA was extracted to capture RNA viruses as well as other pathogens. The RNA was pooled as presumed CCD-positive, presumed CCD-negative, and royal jelly for pyrosequencing. The raw sequencing reads were trimmed and assembled into contiguous sequences (contigs) (fig. S2). Analysis using nucleotide-nucleotide BLAST (BLASTN) and BLASTX (*8*) revealed the presence of bacteria, fungi, parasites, metazoa, and viruses (Table 1).

Sequences homologous to bacterial 16S ribosomal RNA (16S rRNA) were assembled into 48 contigs. The majority (87%) of the contigs aligned best to previously identified commensals of *A. mellifera* (Table 1). To obtain precision in typing the bacterial associates in the different samples, we obtained ~500-nucleotide (nt) fragments of the 16S rRNA gene, using conserved, near-universal PCR primers. A total of 536 clones from the entire range of samples were characterized by conventional sequencing. When these sequences were used as queries in BLASTN searches of GenBank, over 96% gave closest hits to the eight clusters isolated from *A. mellifera* in previous studies (*9*–*11*). These clusters included an abundant member of the Gammaproteobacteria and several less frequent but widespread organisms from the Betaproteobacteria, Alphaproteobacteria, Firmicutes, and Actinobacteria groups (Fig. 1). Only 20 bacterial 16S rRNA gene sequences were unidentified, and they were not concentrated in CCD samples. Sequences of *Paenibacillus larvae* and *Streptococcus pluton*, the causative agents of American and European foulbrood (diseases of bee larvae) were not detected.

Bacterial analysis indicated community composition (Table 1) similar to that in samples collected in Africa, Switzerland, and Germany (*9*–*11*), suggesting that *A. mellifera* has similar bacterial flora worldwide. Screens of the *A. mellifera* genome-sequence database revealed sequences corresponding to several of these bacterial groups, indicating that they are probably part of the normal flora. The *A. mellifera* database includes sequences for 926 genes with significant reciprocal best BLAST hits to genes from completely sequenced bacterial genomes. The most abundantly represented groups corresponded to taxa in our samples, including 299 (32%) with best hits to *Lactobacillus* species and 249 (27%) with best hits to *Neisseria* species (members of the Betaproteobacteria and closest relatives of *Simonsiella* for which screening was possible on the basis of the available full genome sequences). The gut lumen contains the majority of microorganisms in most insects. Because a similar profile of bacterial types was found in dissected intestines from *A. mellifera* (*9*, *11*), the bacterial species described here probably represent a characteristic gut-inhabiting community. Although we cannot exclude that a strain of a normally commensal bacterium has become pathogenic while retaining a near-identical 16S rRNA sequence, we observed no clear shift in abundance to suggest that this occurred in CCD. A trend toward increased abundance of one of the Gammaproteobacterial taxa in the CCD bees (Fig. 1) may reflect physiological changes accompanying CCD and affecting the commensal community. More sampling of individual colonies and age classes would be needed to determine the importance of this observation.

Metagenomic sequence data for a ~700-nt fragment of the 18S rRNA gene identified a trypanosomatid sequence. This sequence was identical across CCD and non-CCD samples. Phylogenetic analysis indicates that this parasite falls in the *Leptomonas-Leishmania-Crithidia* lineage, but a precise taxonomic assignment is not possible because of the paucity of rRNA data in this region (fig. S3) (*12*–*14*).

Eighty-one distinct fungal 18S rRNA sequences were recovered from the pooled samples, primarily from four distinct lineages: Saccharomycotina, which includes a variety of presumed commensal yeasts; Microsporidia, including the important bee pathogens *Nosema apis* and *Nosema ceranae* (*15*); Entomophtorales/Entomphthoromycotina, a diverse group of insect pathogens; and Mucorales/Mucoromycotina, which includes *Mucor hiemalis*, a species known to kill honey bees under certain

Table 1. Closest sequenced relatives identified through BLAST analysis of the high-throughput sequence data.

Kingdom	Taxon (rank)	Organism
Bacteria	Firmicutes (phylum)	*Lactobacillus* sp.*†
		Uncultured Firmicutes†
Bacteria	Actinobacteria (class)	*Bifidobacterium* sp.*
Bacteria	Alphaproteobacteria (class)	*Bartonella* sp.*†
		Gluconacetobacter sp.*†
Bacteria	Betaproteobacteria (class)	*Simonsiella* sp.*†
Bacteria	Gammaproteobacteria (class)	Two uncultured species*†
Fungus	Entomophthorales (order)	*Pandora delphacis*
Fungus	Mucorales (order)	*Mucor* spp.
Fungus/microsporidian	Nosematidae (family)	*Nosema ceranae*
Fungus/microsporidian	Nosematidae (family)	*Nosema apis*
Eukaryota	Trypanosomatidae (family)	*Leishmania/Leptomonas* sp.
Metazoan	Varroidae (family)	*Varroa destructor*
Virus	(Unclassified)	CBPV‡
Virus	*Iflavirus* (genus)	SBV
Virus	*Iflavirus* (genus)	DWV‡
Virus	Dicistroviridae (family)	BQCV
Virus	Dicistroviridae (family)	KBV‡
Virus	Dicistroviridae (family)	ABPV
Virus	Dicistroviridae (family)	IAPV of bees‡

*Found by Jeyaprakash *et al*. (*10*). †Found by Babendreier *et al*. (*9*). ‡Indicates viruses not yet classified by the International Committee on the Taxonomy of Viruses but that exhibit the key features of the indicated taxon.

[1]Department of Entomology, Pennsylvania State University, University Park, PA 16802, USA. [2]Center for Infection and Immunity, Mailman School of Public Health, Columbia University, New York, NY 10032, USA. [3]Center for Infectious Disease Dynamics, Department of Biology, Pennsylvania State University, Mueller Laboratory, University Park, PA 16802, USA. [4]Fogarty International Center, National Institutes of Health, Bethesda, MD 20892, USA. [5]Bee Research Laboratory, U. S. Department of Agriculture–Agricultural Research Service, Beltsville, MD 20705, USA. [6]Department of Ecology and Evolutionary Biology, University of Arizona, Tucson, AZ 85721, USA. [7]Department of Plant Pathology, Pennsylvania State University, University Park, PA 16802, USA. [8]Center for Insect Science, University of Arizona, Tucson, AZ 85721, USA. [9]Pennsylvania Department of Agriculture, Bureau of Plant Industry–Apiculture, Harrisburg, PA 17110, USA. [10]454 Life Sciences, Branford, CT 06405, USA.

*To whom correspondence should be addressed. E-mail: wil2001@columbia.edu

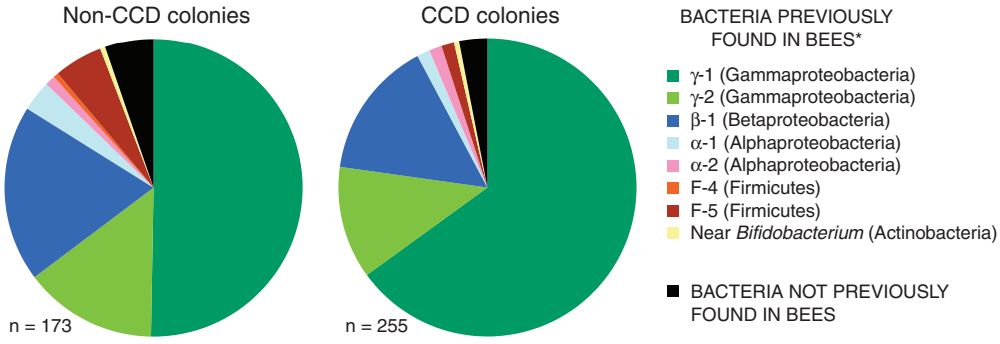

Fig. 1. Summary of bacterial groups from *A. mellifera* derived from colonies categorized as non-CCD and CCD. For both categories, the top BLAST hit for over 96% of sequences from 16S rRNA clones was a sequence obtained in previous studies on bacterial associates of *A. mellifera*. Asterisk indicates that the bacteria were categorized according to the cluster designations of Babendreier *et al*. (*9*) [except for the Bifidobacterium-like sequence of Jeyaprakash *et al*. (*10*)]. *n*, number of sequences. GenBank accession numbers corresponding to the categories are: γ-1 (AY370191-AY370192 and DQ837602-DQ837609), γ-2 (DQ837610-DQ837611), β-1 (AY370189-AY370190 and DQ837616-DQ837621), α-1 (AY370185-AY370187 and DQ837622-DQ837624), α-2 (AY370188 and DQ837625-DQ837626), F-4 (DQ837632-DQ837633), F-5 (AY370183 and DQ837634-DQ837637), near Bifidobacterium (AY370184).

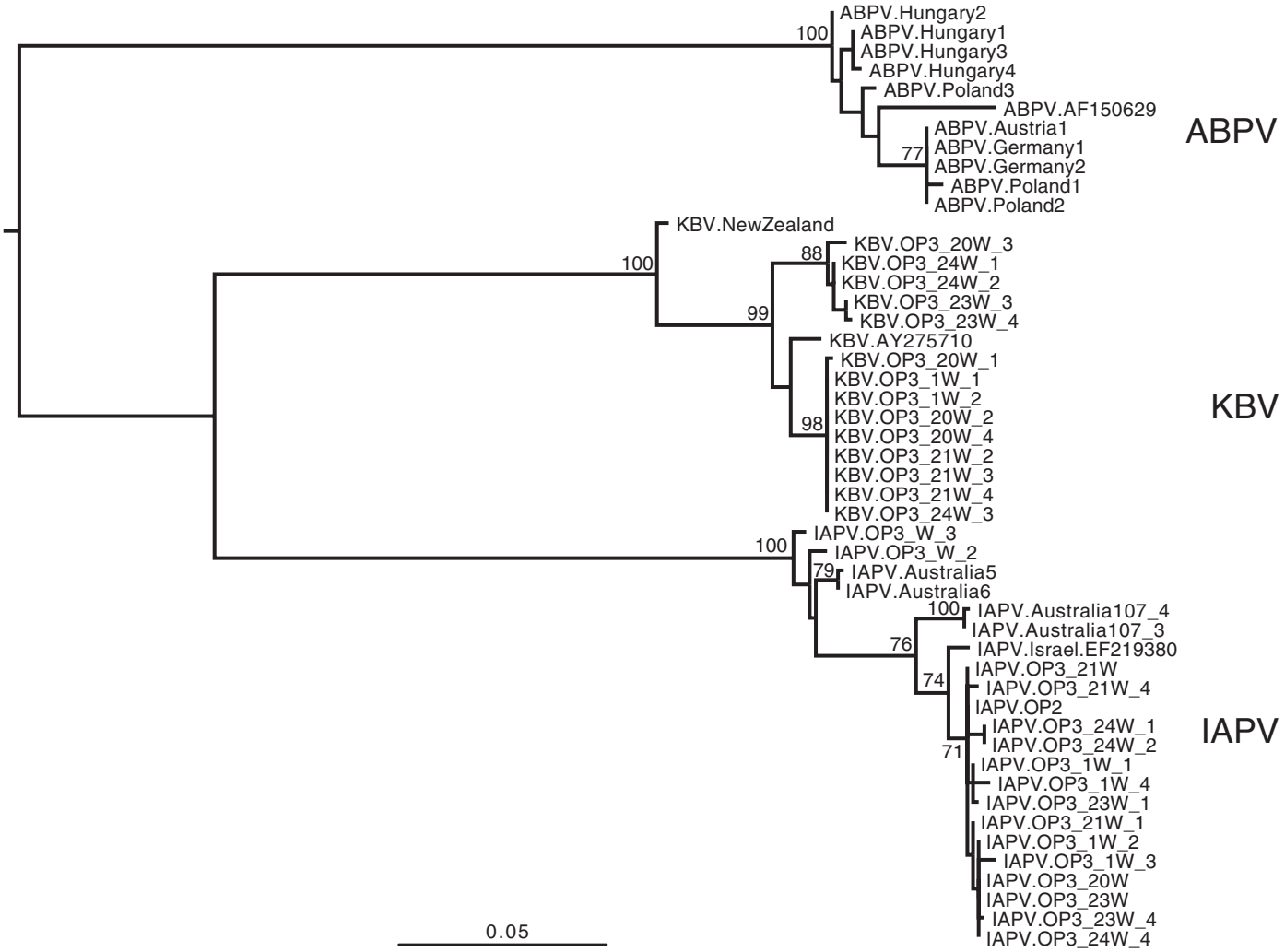

Fig. 2. Maximum likelihood phylogenetic tree of dicistroviruses, based on a 741-nt sequence including the IGR. All branches are drawn to a scale of substitutions per site, and bootstrap values are shown for key nodes. All KBV sequences (except KBV.NewZealand and KBV.AY275710) and all IAPV sequences (except IAPV.Israel.EF219380) were recovered in this study. 0.05 represents the number of nucleotide substitutions per site. GenBank accession numbers for the nucleotide sequences in file IAPVaug07IGR.sqn: IAPV.Australia107_4 EU122346, IAPV.Australia5 EU122347, IAPV.Australia6 EU122348, IAPV.Australia107_3 EU122349, IAPV.OP3_1W_1 EU122350, IAPV.OP3_1W_2 EU122351, IAPV.OP3_1W_3 EU122352, IAPV.OP3_1W_4 EU122353, IAPV.OP3_20W EU122354, IAPV.OP3_21W EU122355, IAPV.OP3_21W_1 EU122356, IAPV.OP3_W_2 EU122357, IAPV.OP3_W_3 EU122358, IAPV.OP3_21W_4 EU122359, IAPV.OP3_23W EU122360, IAPV.OP3_23W_1 EU122361, IAPV.OP3_23W_4 EU122362, IAPV.OP3_24W_1 EU122363, IAPV.OP3_24W_2 EU122364, IAPV.OP3_24W_4 EU122365, IAPV.OP2 EU122366, KBV.OP3_20W_1 EU122367, KBV.OP3_1W_1 EU122368, KBV.OP3_1W_2 EU122369, KBV.OP3_20W_2 EU122370, KBV.OP3_20W_3 EU122371, KBV.OP3_20W_4 EU122372, KBV.OP3_21W_2 EU122373, KBV.OP3_21W_3 EU122374, KBV.OP3_21W_4 EU122375, KBV.OP3_23W_3 EU122376, KBV.OP3_23W_4 EU122377, KBV.OP3_24W_1 EU122378, KBV.OP3_24W_2 EU122379, KBV.OP3_24W_3 EU122380.

conditions (*16*). We used 18S rRNA PCR primers designed to capture Entomophthorales and Mucorales (fig. S4). The occurrence of these fungi in our samples did not correlate with CCD (table S1). Although *N. ceranae* was detected by PCR in all operations affected by CCD, as well as in the Australian sample and two of the royal-jelly samples, it was also detected in non-CCD samples. A specific PCR assay for *N. apis* showed that it was present in all four CCD operations, as well as one non-CCD operation. *N. apis* was also found in the sample from Australia but not in the royal-jelly samples (table S1).

BLASTN analysis of the high-throughput sequencing data identified seven positive-sense single-stranded RNA viruses previously associated with disease in honey bees, including members of the family Dicistroviridae and the genus *Iflavirus*. The presence of the unclassified Chronic bee paralysis virus (CBPV) in only one out of four CCD operations (table S1) suggests that it is not a primary contributor to this syndrome. Recovered sequences were used to establish specific quantitative PCR assays for the remaining six insect viruses. Two iflaviruses, Sacbrood virus (SBV) and Deformed wing virus (DWV), as well as two dicistroviruses, Black queen cell virus (BQCV) and Acute bee paralysis virus (ABPV), were found in both CCD and non-CCD operations.

Two other dicistroviruses, Kashmir bee virus (KBV) and Israeli acute paralysis virus (IAPV) of bees—an unclassified virus that may reflect a distinct lineage of KBV or a previously unidentified species—were found only in CCD operations. IAPV sequence analysis in the intergenic region (IGR) (Fig. 2) indicated a close phylogenetic relation to both KBV and ABPV. IAPV was found in all four affected operations sampled, in two out of four royal-jelly samples, and in the Australian sample (table S1). KBV was present in three out of four CCD operations but not in the royal jelly. KBV was not found in the sample of Australian bees shown in table S1; however, KBV was subsequently found in five out of eleven individual bees from the same Australian source.

Both *N. ceranae* and an unspecified iflavirus were proposed to be associated with CCD in an earlier report (*17*). We found *Nosema* spp. by PCR and spore count in both CCD and non-CCD operations (tables S1 and S2) but no novel iflavirus. The overall prevalence of any *Nosema* species was 94.1% (100%, CCD; 85.7%, non-CCD). In contrast, the dicistroviruses KBV and IAPV correlated with CCD in our metagenomic survey. The prevalence of KBV, IAPV, *N. ceranae*, and *N. apis* was tested in 51 pools of bees (4 to 15 bees per pool) collected from 30 CCD colonies and 21 non-CCD colonies between 2004 and 2007 in Arizona, California, Florida, Georgia, Louisiana, and Pennsylvania. Individual CCD samples were more likely than samples from non-CCD operations to contain more than one of these four pathogens. The mean number of pathogen types (±1 SD) found in individual samples from each site was 3.7 ± 0.5 for CCD samples versus 2.1 ± 0.9 for non-CCD samples ($P < 0.0001$). The patterns of coinfection were complex and unevenly distributed throughout the sample set. All samples that were positive for IAPV also contained KBV. Although KBV was prevalent in both CCD and non-CCD samples (90.2% of all samples), IAPV was, with a single exception, confined to CCD samples, yielding a positive predictive value of 96.1% and a specificity of 95.2% (Table 2). Multinomial logistic regression was pursued to determine the contributions of the four pathogens, singly and in combination, to CCD outcomes. Models with the best explanatory power included IAPV as one of the independent variables. IAPV was found to increase the risk of CCD (odds ratio = 65, $P < 0.0001$) with a trend for increased CCD risk in samples positive for *N. apis* (odds ratio = 9, $P = 0.053$). Neither KBV nor *N. ceranae* contributed significantly to the risk for CCD, nor did they alter the influence of IAPV on CCD.

IAPV was first described in 2004 in Israel (*18*) where infected bees presented with shivering wings, progressed to paralysis, and then died just outside the hive. All of the CCD operations that were sampled used imported bees from Australia or were intermingled with operations that had done so. Importation to the United States of bees from Australia began in 2004, coinciding with early reports of unusual colony declines. Although the shivering phenotype is not reported in imported Australian bees or CCD, differences in IAPV pathogenicity may reflect strain variation, coinfection, or the presence of other stressors such as pesticides or poor nutrition. The varroa mite, for example, which is absent in Australia, immunosuppresses bees, making them more susceptible to infection by other organisms, including viruses (*19*, *20*). Other stressors may include chemical pesticides used on plants pollinated by bees and in hives to control pests. Crop pesticide use is similar in both the United States and Australia. Miticides are widely used in the United States but not in Australia and can have adverse effects on colony health (*21*); however, miticide use did not differ between CCD and non-CCD operations, as determined by detailed case histories (*22*).

We used CCD as a model to establish a strategy for investigating epidemics of unexplained infectious disease. Metagenomic sequencing enabled rapid assembly of a comprehensive inventory of microflora in CCD and non-CCD populations and provided the foundation needed to address the significance and provenance of candidate pathogens. We have not proven a causal relationship between any infectious agent and CCD; nonetheless, the prevalence of IAPV sequences in CCD operations, as well as the temporal and geographic overlap of CCD and the importation of IAPV-infected bees, indicate that IAPV is a significant marker for CCD.

Table 2. Analysis of pools of bees tested for candidate pathogens. Numbers in the CCD, Non-CCD, and Total columns represent the percentage of samples found to be positive among all samples tested in each category. The positive predictive value represents the probability that a positive result for a given agent is associated with CCD. The sensitivity is the probability that test results will be positive in all CCD cases. Specificity is defined as the probability that all non-CCD samples will be associated with negative test results.

Agent	CCD (n = 30)	Non-CCD (n = 21)	Total (n = 51)	Positive predictive value (%)	Sensitivity (%)	Specificity (%)
IAPV	25 (83.3%)	1 (4.8%)	26 (51.0%)	96.1	83.3	95.2
KBV	30 (100%)	16 (76.2%)	46 (90.2%)	65.2	100	23.8
N. apis	27 (90%)	10 (47.6%)	37 (72.5%)	73.0	90.0	52.4
N. ceranae	30 (100%)	17 (80.9%)	47 (92.1%)	63.8	100	19.0
All four agents	23 (76.7%)	0 (0%)	23 (45.0%)	100	76.7	100

References and Notes

1. M. Margulies *et al.*, *Nature* **437**, 376 (2005).
2. B. P. Oldroyd, *PLoS Biol.* **5**, e168 (2007).
3. A. Barrionuevo, "Bees vanish; Scientists race for reasons," *New York Times*, 24 April 2007, p. 1.
4. E. Stokstad, *Science* **316**, 970 (2007).
5. D. vanEngelsdorp, R. Underwood, D. Caron, J. Hayes Jr., *Am. Bee J.* **147**, 599 (2007).
6. J. Pettis, D. vanEngelsdorp, D. Cox-Foster, *Am. Bee J.* **147**, 595 (2007).
7. Materials and methods are available as supporting material on *Science* Online.
8. S. F. Altschul *et al.*, *Nucleic Acids Res.* **25**, 3389 (1997).
9. D. Babendreier, D. Joller, J. Romeis, F. Bigler, F. Widmer, *FEMS Microbiol. Ecol.* **59**, 600 (2007).
10. A. Jeyaprakash, M. A. Hoy, M. H. Allsopp, *J. Invertebr. Pathol.* **84**, 96 (2003).
11. K. I. Mohr, C. C. Tebbe, *Environ. Microbiol.* **8**, 258 (2006).
12. S. Podlipaev, *Int. J. Parasitol.* **31**, 648 (2001).
13. S. A. Podlipaev *et al.*, *J. Eukaryot. Microbiol.* **51**, 283 (2004).
14. A. L. Hughes, H. Piontkivska, *Mol. Biol. Evol.* **20**, 644 (2003).
15. M. Higes, R. Martin, A. Meana, *J. Invertebr. Pathol.* **92**, 93 (2006).
16. C. E. Burnside, *Am. Bee J.* **25**, 75 (1935).
17. W. Ravven, "UCSF sleuths identify suspects in mystery of vanishing honeybees," *UCSF Today*, 25 April 2007; available at http://pub.ucsf.edu/today/cache/feature/200704251.html.
18. E. Maori, E. Tanne, I. Sela, *Virology* **362**, 342 (2007).
19. X. Yang, D. L. Cox-Foster, *Proc. Natl. Acad. Sci. U.S.A.* **102**, 7470 (2005).
20. P. G. Gregory, J. D. Evans, T. Rinderer, L. de Guzman, *J. Insect Sci.* **5**, 7 (2005).
21. J. Pettis, A. Collins, R. Wilbanks, M. F. Feldlaufer, *Apidologie* **35**, 605 (2004).
22. D. vanEngelsdorp, D. Cox-Foster, M. Frazier, N. Ostiguy, J. Hayes Jr., "Fall-Dwindle Disease: A preliminary report" (CCD Working Group, 2006); available at http://maarec.cas.psu.edu/ColonyCollapseDisorderInfo.html.

23. We thank M. Andree, A. V. Bussetti, J. Chen, D. Grove, M. Hamilton, V. Levi, H. Lin, D. Lopez, S. McDonald, N. Rice, K. Roccasecca, B. Smith, O. Thompson, A. Ulsamer, V. Williams, and the beekeepers who supplied the samples used in these analyses. The work reported here was supported by NIH awards U01AI070411 and U54AI57158 (Northeast Biodefense Center-Lipkin), the National Honey Board, and the Pennsylvania Department of Agriculture.

Supporting Online Material
www.sciencemag.org/cgi/content/full/1146498/DC1
Materials and Methods
Figs. S1 to S4
Tables S1 to S3
References

14 June 2007; accepted 30 August 2007
Published online 6 September 2007;
10.1126/science.1146498
Include this information when citing this paper

Coactivation of Receptor Tyrosine Kinases Affects the Response of Tumor Cells to Targeted Therapies

Jayne M. Stommel,[1] Alec C. Kimmelman,[1,2] Haoqiang Ying,[1] Roustem Nabioullin,[3] Aditya H. Ponugoti,[3] Ruprecht Wiedemeyer,[1] Alexander H. Stegh,[1] James E. Bradner,[4] Keith L. Ligon,[1,5] Cameron Brennan,[6] Lynda Chin,[1,3,7] Ronald A. DePinho[1,3,8]*

Targeted therapies that inhibit receptor tyrosine kinases (RTKs) and the downstream phosphatidylinositol 3-kinase (PI3K) signaling pathway have shown promising anticancer activity, but their efficacy in the brain tumor glioblastoma multiforme (GBM) and other solid tumors has been modest. We hypothesized that multiple RTKs are coactivated in these tumors and that redundant inputs drive and maintain downstream signaling, thereby limiting the efficacy of therapies targeting single RTKs. Tumor cell lines, xenotransplants, and primary tumors indeed show multiple concomitantly activated RTKs. Combinations of RTK inhibitors and/or RNA interference, but not single agents, decreased signaling, cell survival, and anchorage-independent growth even in glioma cells deficient in PTEN, a frequently inactivated inhibitor of PI3K. Thus, effective GBM therapy may require combined regimens targeting multiple RTKs.

GBM, the most prevalent tumor in the central nervous system of human adults, is among the most lethal cancers, with a median survival of ~12 months (*1*). Aberrant activation of PI3K pathway components appears to be universal in human cancer, including GBM. PI3K is activated upon binding phosphorylated RTKs and/or adaptor proteins at the plasma membrane and signals to multiple downstream effectors, such as Akt (*2*). Over 80% of GBMs show robust Akt activation, and 40 to 50% have lost or mutated PTEN (*3*), underscoring the importance of the PI3K pathway in gliomagenesis (*4*). Activation of the RTK epidermal growth factor receptor (EGFR) is a critical pathogenetic event, with amplification, mutation, and rearrangement observed in more than 40% of cases, making it a compelling target for therapeutic inhibition (*5*, *6*). Other RTKs, such as the platelet-derived growth factor receptors α and β (PDGFRα and PDGFRβ) and MET (*1*, *7*), have been reported to be altered in GBM, albeit at lower frequencies. Notably, anti-PDGFR therapy has failed in GBM patients (*8*), and only 10 to 20% of patients benefit from EGFR inhibition (*9*), pointing to confounding factors that attenuate the response to RTK inhibition.

Coexpression of wild-type (WT) PTEN and a constitutively active EGFR (vIII mutant) in GBM correlates with clinical response to EGFR inhibitors, indicating that PTEN is a response biomarker for anti-EGFR therapy and that its loss renders these agents ineffective by dissociating EGFR inhibition from the abrogation of PI3K pathway activity (*10*). Alternatively, the activation state of critical survival pathways, such as PI3K and mitogen-activated protein kinase (MAPK), may be determined by the sum of multiple inputs, and multiple RTKs besides EGFR may be simultaneously or sequentially used by GBM cells to maintain signal flux through such pathways. In such a multiple-input system, single-agent anti-EGFR inhibition might be incapable of sufficiently suppressing PI3K signaling in the context of unopposed activation by PTEN loss, resulting in a lack of clinical efficacy. That is, the total signal flux through the PI3K pathway may dictate the response to upstream RTK inhibition, and multiple inputs to PI3K signaling would thus confer insensitivity to the inhibition of any single agent.

To evaluate this possibility, we sought evidence that multiple PI3K activators coexist in glioma cells (*11*). Because PI3K is activated by binding phosphorylated proteins to its regulatory subunit, p85α, we performed anti-p85α immunoprecipitations to identify PI3K-activating proteins. Multiple tyrosine-phosphorylated proteins were found to be in the PI3K complex (fig. S1A). Guided by Scansite [http://scansite.mit.edu (*12*)], which identifies potential p85α-binding proteins, we confirmed the endogenous PI3K interaction with specific RTKs by coimmunoprecipitation assays. For example, 5 out of 14 cell lines showed activated ERBB3 (fig. S1B), which mediates the binding of EGFR and ERBB2 to PI3K (*13*), and 9 out of 20 cell lines had activated growth factor receptor–bound protein 2 (Grb2)–associated binder 1 (GAB1), a docking protein that binds activated RTKs directly or through Grb2 (*14*). In seven of these 20 cell lines, highly phosphorylated GAB1 coimmunoprecipitated activated MET (fig. S2B) (*15*).

To define the compendium of coactivated RTKs in GBM, we used an antibody array that allows simultaneous assessment of the phosphorylation status of 45 RTKs. Consistent with figs. S1 and S2, three or more activated RTKs, including EGFR, ERBB3, PDGFRα, and MET, were detected in each of 19 out of 20 cell lines (Fig. 1A and table S1). Most activated RTKs remained phosphorylated under serum deprivation and in tumor cell xenografts (Fig. 1, B and C), indicating that the RTK activation in the transformed cells is not due to ligands in serum-containing culture media. Finally, RTK coactivation is not a distinctive feature of glioma cells, because similar patterns were detected in other solid tumor types such as lung and pancreatic adenocarcinoma cell lines (fig. S3).

To explore the therapeutic implications of RTK coactivation, we used U87MG glioma cells that constitutively express WT EGFR, EGFRvIII (EGFR*), or a kinase-dead EGFRvIII (EGFR*-KD) at levels comparable to those observed in primary GBMs (*16*). Although MET is phosphorylated and bound to GAB1 in U87MG cells (Fig. 2A and fig. S2B), activated MET was substantially displaced by EGFR in the GAB1/PI3K complex when WT EGFR and EGFR* are expressed. This outcome required the catalytic activity of EGFR, because EGFR*-KD only modestly displaced MET (lane 4 in Fig. 2A). Because EGFR*-KD was expressed at levels similar to those of WT EGFR and EGFR*, it is unlikely that the displacement was simply a consequence of ectopic overexpression. This apparent "swapping" of RTKs within the PI3K

[1]Department of Medical Oncology, Dana-Farber Cancer Institute and Harvard Medical School, Boston, MA 02115, USA. [2]Harvard Radiation Oncology Program, Harvard Medical School, Boston, MA 02115, USA. [3]Center for Applied Cancer Science, Belfer Institute for Innovative Cancer Science, Dana-Farber Cancer Institute, Boston, MA 02115, USA. [4]Division of Hematologic Neoplasia, Dana-Farber Cancer Institute and Harvard Medical School, Boston, MA 02115, USA. [5]Department of Pathology, Division of Neuropathology, Brigham and Women's Hospital, Boston, MA 02115, USA. [6]Departments of Neurosurgery, Memorial Sloan Kettering Cancer Center and Neurological Surgery, Weill Medical College of Cornell University, New York, NY 10021, USA. [7]Department of Dermatology, Brigham and Women's Hospital and Harvard Medical School, Boston, MA 02115, USA, [8]Departments of Medicine and Genetics, Harvard Medical School, Boston, MA 02115, USA.

*To whom correspondence should be addressed. E-mail: ron_depinho@dfci.harvard.edu